Catalysts **2011**, *1*, 18-39; doi:10.3390/catal1010018

OPEN ACCESS

catalysts

ISSN 2073-4344

www.mdpi.com/journal/catalysts

Article

Role of the Support Effects on the Catalytic Activity of Gold Clusters: A Density Functional Theory Study

Min Gao [1], Andrey Lyalin [1,2,⋆] and Tetsuya Taketsugu [1]

[1] Division of Chemistry, Graduate School of Science, Hokkaido University, Sapporo 060-0810, Japan; E-Mails: gaomin1986@gmail.com (M.G.); take@sci.hokudai.ac.jp (T.T.)

[2] V. A. Fock Institute of Physics, St Petersburg State University, Petrodvorez 198504, Russia

⋆ Author to whom correspondence should be addressed; E-Mail: lyalin@mail.sci.hokudai.ac.jp; Tel.: +81-0-80-3292-3010; Fax: +81-0-11-706-4921.

Received: 6 October 2011; in revised form: 31 October 2011 / Accepted: 16 November 2011 / Published: 17 November 2011

Abstract: It is demonstrated that the support effects play a crucial role in the gold nanocatalysis. Two types of support are considered—the "inert" support of hexagonal boron nitride (h-BN) with the N and B vacancy defects and the "active" support of rutile TiO_2(110). It is demonstrated that Au and Au_2 can be trapped effectively by the vacancy defects in h-BN. In that case, the strong adsorption on the surface defects is accompanied by the charge transfer to/from the adsorbate. The excess of the positive or negative charge on the supported gold clusters can considerably promote their catalytic activity. Therefore gold clusters supported on the defected h-BN surface can not be considered as pseudo-free clusters. We also demonstrate that the rutile TiO_2(110) support energetically promotes H_2 dissociation on gold clusters. We show that the formation of the OH group near the supported gold cluster is an important condition for H_2 dissociation. We demonstrate that the active sites towards H_2 dissociation on the supported Au_n are located at corners and edges of the gold cluster in the vicinity of the low coordinated oxygen atoms on TiO_2(110). Thus catalytic activity of a gold nanoparticle supported on the rutile TiO_2(110) surface is proportional to the length of the perimeter interface between the nanoparticle and the support.

Keywords: nanocatalysis; gold clusters; support effect; interface effect; oxygen activation; hydrogen dissociation

1. Introduction

Since the pioneering work of Haruta on the oxidation of carbon monoxide on small gold nanoparticles supported by metal oxides [1], an extensive interest has been devoted to understanding the catalytic properties of gold. Such an interest is stipulated by the fact that gold nanoparticles are catalytically active even at room temperatures and demonstrate extraordinary selectivity. This feature makes gold clusters very attractive for a wide range of industrial, chemical and environmental applications [2–4].

Two types of catalytic reactions on gold nanoparticles—oxidation by O_2 and hydrogenation by H_2—are extremely important for applications. The most explored types of oxidation reaction include the oxidation of carbon monoxide at mild temperatures, alcohol oxidation, the direct synthesis of hydrogen peroxide and alkene epoxidation; see, e.g., References [1,5–11] and references therein. Heterogeneously catalyzed hydrogenation is another type of reactions where gold nanoparticles have shown their great potential as catalysts. It has been demonstrated experimentally that gold nanoparticles supported on metal oxides such as SiO_2, Al_2O_3, TiO_2, ZnO, ZrO_2, and Fe_2O_3 are effective catalysts for selective hydrogenation of several classes of organic molecules, including α, β-unsaturated aldehydes, unsaturated ketones, and unsaturated hydrocarbons [12–21]. Moreover, supported gold nanoparticles are very selective for the direct formation of hydrogen peroxide from H_2/O_2 mixtures [9].

In spite of intensive theoretical and experimental studies the origin of catalytic activity of gold nanoparticles remains elusive and has yet to be fully understood. It is commonly accepted that several factors can influence the catalytic activity of gold nanoparticles. One of them is the size effect. It has been shown that the unique properties of gold in oxidation reactions emerge when the size of catalytic particles decreases down to 1–5 nm, while larger sized particles are catalytically inactive [5]. It has been shown that small gold clusters consisting of a few atoms can also possess extraordinarily high catalytic activity [22,23]. This is the regime where each atom counts, physical and chemical properties of clusters are extremely size sensitive and cannot be deduced from those known for larger sizes [4,24,25]. On the one hand, the size effects in nanocatalysis are determined by quantum effects, resulting from the spatial confinement of the valence electrons in the cluster [4]; on the other hand, in such clusters a dominant fraction of atoms are under-coordinated (in comparison with the bulk), hence they exhibit an enhanced chemical reactivity [4,26,27].

The charge state of the gold nanoparticles can considerably influence their reactivity [11,28]. For example, in the case of the negatively charged gold nanoparticles, an extra electron from the gold readily transfers to the anti-bonding $2\pi^*$ orbital of the adsorbed O_2, which weakens the O–O bond and activates oxygen molecule for further catalytic reaction; see, e.g., References [10,11,29–31] and references therein. Such mechanism of the charge-transfer-mediated activation of O_2 by gold clusters has been intensively studied [32–35]. On the other hand, the positive charge accumulated on the gold can promote adsorption of some reactants, such as CO and hydrocarbons [36,37].

Interaction with the support material is another important factor that considerably influences the reactivity of gold nanoparticles [4,38]. Most of the experimental studies have been performed for gold nanoparticles supported on various metal oxides, such as MgO, ZnO, TiO_2, ZrO_2, Al_2O_3, Fe_2O_3, see, e.g., Reference [2] and references therein. It was demonstrated that the catalytic activity of gold nanoparticles strongly depends on the type of the support material [2,5,39]. Often, an electron transfer

from the support to the gold cluster promotes its catalytic activity because it opens a route for an extra charge transfer to the adsorbed O_2. Catalytic activity of the supported nanoparticles can also be promoted by defects in the support material. Defects can trap the metal nanoparticle and enhance charge transfer between the support and the nanoparticle. Thus, it was demonstrated that Au_8 clusters supported on the MgO(100) surface rich of F-center defects show high catalytic activity, while Au_8 deposited on the defect-poor MgO(100) surface are inert [40,41]. Defects are not the only factor responsible for charging of the supported metal nanoparticles. Recently, it was demonstrated that the charge accumulated on the supported gold nanoparticle can be tuned by varying the thickness of the metal oxide layer deposited on the metal support [42–46]. Thus, the support effects can play even larger role in gold nanocatalysis than the particle size.

In the present work we demonstrate that the charge transfer from the support to the deposited gold clusters is not the only mechanism responsible for the promotion of the cluster's catalytic activity. Two types of support will be considered—the hexagonal boron nitride (h-BN) with N and B vacancy defects and the rutile TiO_2(110). Using these two examples we show that the support effects on the catalytic activity of gold clusters can be rather diverse and can have different origins.

It is commonly accepted that "inert" supports, such as, h-BN do not affect the electronic and geometric structure of the supported clusters, and hence such clusters can be considered as pseudo-free. This suggestion is widely used to study intrinsic properties of metal clusters that are free from the support effects [6]. Indeed, h-BN is an electrical insulator with a wide band gap ($\sim$5.8 eV) and high thermal and chemical stability [47,48]. It is unlikely that such a support can promote an electron transfer to or from the deposited gold nanoparticle and influence their physical and chemical properties.

Recently, it has been demonstrated experimentally that small gold clusters deposited on h-BN support are efficient and robust catalysts [6]. However, very little attention has been paid to theoretical investigations concerning the role of the h-BN support on the catalytic properties of gold. Whether the origin of catalytic activity of gold clusters supported on h-BN surface derives from the cluster itself, or h-BN support can modify or tune catalytic properties of gold?

Contrary to the case of the "inert" h-BN support, the rutile TiO_2(110) surface is considered as an active surface that can even possess catalytic properties itself. It has been found experimentally that catalytic activity of gold nanoparticles supported on the rutile TiO_2(110) surface towards H_2 dissociation depends on the number of gold atoms located at the perimeter nanoparticle-support interface, irrespective of the cluster size [38]. It has been also shown that the active sites for the H_2 + O_2 reaction over a Au/TiO_2 nanoparticle catalyst are located at dual perimeter sites at the interface between Au and TiO_2 [49]. To the best of our knowledge there are only few theoretical studies concerning the role of the support on the processes of adsorption and dissociation of molecular hydrogen on the supported gold nanoparticles [50–52]. In Reference [50] the authors performed an elegant theoretical study on elucidation of active sites for H_2 adsorption and activation on Au_{13} cluster supported on the anatase TiO_2(001) surface. It has been shown that Au atoms that are active for H_2 dissociation must have a net charge close to zero, be located at corner or edge low coordinated positions, and not be directly bonded to the support [50]. An important role of the low coordinated oxygen atoms at the nanoparticle/TiO_2 interface has been discussed [52]. In Reference [51] it was shown that small two-dimensional Au nanoparticles supported on TiC(001) can dissociate H_2 in a more efficient way than when supported

on oxides. The active sites for H_2 dissociation on Au/TiC(001) are located at the particle edge and in direct contact with the underlying substrate [51]. In the present work we clarify how hydrogen molecule adsorbs and dissociates on the supported gold nanoparticles.

We demonstrate that the support effects are very important in the gold nanocatalysis. Even the "inert" h-BN support, if it contains point defects, can promote or quench the catalytic properties of gold in oxidation reaction by O_2. Therefore gold clusters supported on the defected h-BN surface can not be considered as pseudo-free clusters. We demonstrate that rutile $TiO_2(110)$ support energetically promotes H_2 dissociation on gold clusters. We show that the formation of the OH group near the supported gold cluster is an important condition for H_2 dissociation and the conventional charge transfer mechanism does not play an important role for H_2 dissociation. The considered phenomena can be particularly important for understanding the mechanisms of the catalytic activity of the supported gold clusters in oxidation reactions by O_2 and hydrogenation reactions by H_2.

2. Computational Details

The calculations are carried out using density-functional theory (DFT) with the gradient-corrected exchange-correlation functionals of Wu and Cohen (WC) [53] and Perdew, Burke and Ernzerhof (PBE) [54] for O_2Au_n/h-BN and $H_2Au_n/TiO_2(110)$ systems, respectively. The choice of DFT functionals is stipulated by the fact that WC gives significant improvements for lattice constants, crystal structures, and surface energies over the most popular PBE functional, while PBE remains superior for the energetics of covalent and noncovalent bonds [55]. In particular, the PBE functional demonstrates very poor performance for the layered-systems like graphite or h-BN, whose distances between the layers are determined by rather weak interactions [55]. Thus, in the case of h-BN lattice the PBE functional demonstrate only marginal binding of the hexagonal layers along "c", while WC provides very accurate results that are close to experiment [55]. On the other hand PBE can reproduce well the tetragonal rutile TiO_2 structure, and therefore it has been selected to treat $H_2Au_n/TiO_2(110)$ system.

The atom-centered, strictly confined, numerical basis functions [56,57] are used to treat the valence electrons of H ($1s^1$), B ($2s^2 2p^1$), N ($2s^2 2p^3$), O ($2s^2 2p^4$), Ti ($4s^2 3d^2$) and Au ($6s^1 5d^{10}$). Double-ζ plus polarization function (DZP) basis sets are used for B, N, O, Ti, Au and triple-ζ plus polarization function (TZP) for H. Basis set for hydrogen was optimized with the use of the Nelder–Mead simplex method [58] according to the procedure described in Reference [57]. The core electrons are represented by the Troullier–Martins norm-conserving pseudopotentials [59] in the Kleinman-Bylander factorised form [60]. Relativistic effects are taken into account for Au.

In the present work, the h-BN lattice has been optimized using the Monkhorst-Pack [61] $10 \times 10 \times 4$ k-point mesh for Brillouin zone sampling. The calculated lattice parameters a = b = 2.504 Å and c = 6.656 Åare in excellent agreement with the experimental values of a = b = 2.524 $\pm$ 0.020 Å and c = 6.684 $\pm$ 0.020 Å, reported in Reference [62]. The h-BN surface is represented by the two-layer slab containing 7×7 unit cells (98 units of BN per slab) with the surface area of 3.07 nm^2. The bottom layer in the h-BN slab is fixed while the top layer is fully relaxed. The rutile lattice was optimized using the $6 \times 6 \times 9$ k-point mesh. The calculated lattice parameters a = 4.594 Å and c = 2.959 Å are in agreement with the experimental values of a = b = 4.587 Å, c = 2.954 Å at 15 K [63,64]. The optimized lattice of the bulk rutile was used to construct slabs for the $TiO_2(110)$ surface. The six-layer slab containing four

units of TiO_2 represents the element of the (110) rutile face with the surface area of $\sqrt{2}a \times c$. For rutile surface the bottom two layers in the slab are fixed, and all other atoms are fully relaxed. In the present work we study adsorption of Au_n clusters containing n = 1, 2, 8 and 20 atoms on the rutile (110) surface. In the case of Au and Au_2 the TiO_2(110) surface is modeled by the p (2 × 5) slab (40 units of TiO_2 per slab), while for Au_8 and Au_{20} we use p (3 × 6)(72 units of TiO_2) and p (4 × 9)(144 units of TiO_2) slabs, respectively. The periodically replicated slabs for h-BN and TiO_2(110) surfaces are separated by the vacuum region of 25 Å . Only the Γ point is used for sampling the Brillouin zone of the slabs due to the large size of the supercell.

The cluster geometries have been determined with the use of the cluster fusion algorithm [65] which belongs to the class of genetic global optimization methods. This method has been successfully used in order to find the optimized geometries of various types of metal clusters [66–68]. Additionally, the global reaction route mapping (GRRM) technique within the scaled hypersphere search (SHS) method has been used in order to find equilibrium structures [69–71]. The optimized structures of the gold clusters are in a good agreement with those reported in previous theoretical studies; see, e.g., References [30,72–75]. The most stable isomers of gold clusters have been further optimized on the support starting from the several (up to 15) initial orientations and positions of the cluster on the surface.

All calculations have been carried out with the use of the SIESTA package [76–78]. Within the SIESTA approach, the basis functions and the electron density are projected onto a uniform real-space grid. The mesh size of the grid is controlled by an energy cutoff, which defines the wavelength of the shortest plane wave that can be represented on the grid. In the present work the energy cutoff of 200 Ry is chosen to guarantee convergence of the total energies and forces. The self-consistency of the density matrix is achieved with a tolerance of 10^{-4}. For geometry optimization the conjugate-gradient approach was used with a threshold of 0.02 eV $Å^{-1}$. The atoms in molecules method of Bader (AIM) has been used for charge analysis [79,80]. The electron density has been plotted using XCRYSDEN visualisation program [81].

To validate our approach we have calculated the dissociation energies and interatomic distances for several diatomic molecules. Our calculations demonstrate that the dissociation energy, D_e, and bond length in H_2 (4.55 eV, 0.75 Å), O_2 (5.88 eV, 1.24 Å) , Au_2 (2.28 eV, 2.55 Å) are in a good agreement with experimental data H_2 (4.74 eV, 0.74 Å), O_2 (5.23 eV, 1.21 Å), Au_2 (2.29 eV, 2.47 Å)[82]. We also tested the gold–hydrogen interaction by optimizing AuH dimer. The calculated dissociation energy and bond length in AuH (3.09 eV, 1.547 Å) are in a good agreement with experimental data (3.36 eV, 1.524 Å)[82].

3. Theoretical Results

3.1. Adsorption and Activation of O_2 on Au/h-BN and Au_2/h-BN. Role of the Defected h-BN Support

We start our study with investigation of the catalytic activity of small gold clusters supported on the defected hexagonal BN surface. The h-BN lattice has a layered structure which is very similar to graphite. The planar networks of B_3N_3 hexagons are regularly stacks on top of each other [83]. Due to the partially ionic character of the B–N bonding, the B atoms in one layer are located on top of the N atoms of the neighboring layer and vice versa, as it is shown in Figure 1(a). Both graphite and h-BN

materials are strongly bonded within the layers, while interaction between the layers is weak. In spite of similar structures, physical and chemical properties of graphite and h-BN are different. Thus, graphite is an electrical conductor, while h-BN is a dielectric with a wide band gap of 5–6 eV.

Figure 1. h-BN surface models: (**a**) side view of the two-layer h-BN p (7 × 7) slab; (**b**) schematic presentation of the defect-free h-BN surface and h-BN surface with boron (V_B) and nitrogen (V_N) vacancy defects (only part of the top layer is shown).

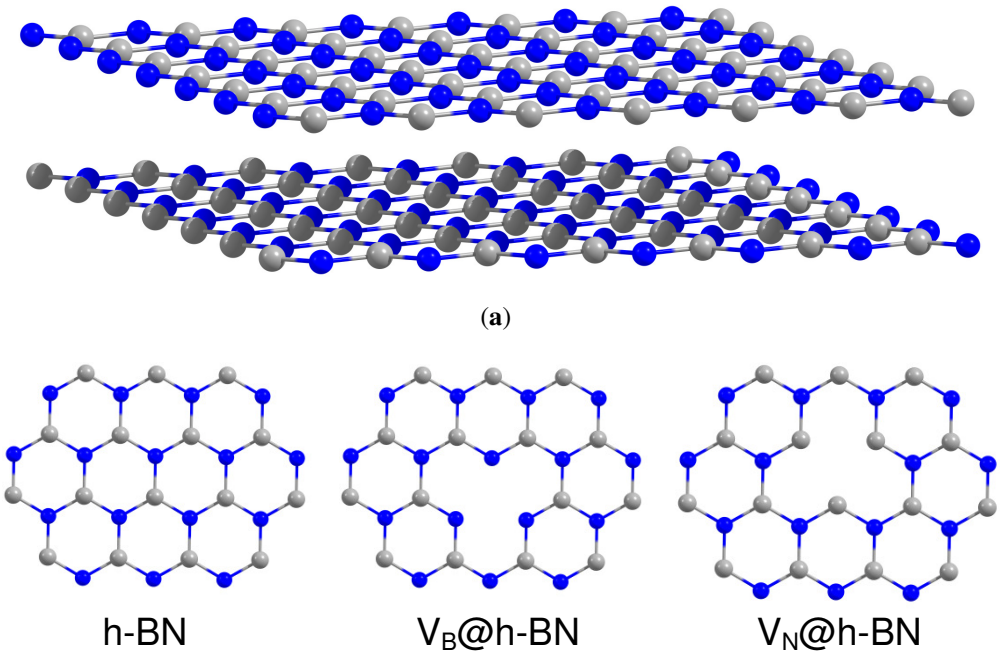

(**a**)

(**b**)

In the present work we study adsorption of gold clusters on the h-BN surface with boron (V_B) and nitrogen (V_N) vacancy defects, which are schematically shown in Figure 1(b). The point V_B and V_N defects are the simplest and relatively stable types of defects in h-BN. It was suggested that single boron and nitrogen vacancy defects can exist in h-BN and V_N is more stable than V_B [84,85]. The stability of divacancies in graphitic boron nitride (g-BN) sheets has been studied in Reference [86]. It was shown that the divacancies are more frequently formed in graphene than in the g-BN [86]; however, it was demonstrated that in BN single-wall nanotubes the most stable type of point defect is the BN divacancy [87]. Formation of the triangle defects in h-BN monolayer has been also investigated; see, e.g., References [88,89] and references therein. It has been demonstrated that N(B) triangle defect states of h-BN atomic layer with N(B) edge atoms have acceptor (donor) levels [89]. A cohesive energy calculation indicates that the h-BN atomic layer with N triangle defects is more or less stable, respectively, than that with B triangle defects when it is negatively or positively charged [89]. The relative stability of particular type of defects in h-BN often depends on the experimental conditions. Therefore, in the present work we study only the simplest types of single point defects, such as V_B and V_N.

Recently, it was demonstrated that h-BN monolayer binds to surfaces of many 3d, 4d, and 5d transition metals, forming the so-called nanomesh structure [90]. The interaction between the h-BN monolayer and transition metal support is mainly driven by mixing of N-p_z and B-p_z orbitals of h-BN monolayer with the

d_{z^2} transition metal orbitals [91]. Similar effect is responsible for bonding of gold clusters to the h-BN surface. In the case of defect-free h-BN surface, both Au and Au_2 adsorb on top of the N atom. Our calculations confirm that Au and Au_2 interact weakly with the pristine h-BN surface. Thus, the calculated binding energies of Au and Au_2 on h-BN are E_b(Au/h-BN) = 0.25 eV and E_b(Au_2/h-BN) = 0.77 eV, respectively. Here, the binding energy of Au and Au_2 to the h-BN surface is defined as

$$E_b(\mathrm{Au}_{1,2}/\mathrm{h{-}BN}) = E_{tot}(\mathrm{Au}_{1,2}) + E_{tot}(\mathrm{h{-}BN}) - E_{tot}(\mathrm{Au}_{1,2}/\mathrm{h{-}BN}) \quad (1)$$

where E_{tot}($Au_{1,2}$/h-BN) denotes the total energy of the $Au_{1,2}$/h-BN system, while E_{tot}($Au_{1,2}$) and E_{tot}(h-BN) are the total energies of the non-interacting Au or Au_2 and h-BN slab, respectively. We also found that there is a little charge transfer from the pristine h-BN surface to the adsorbed gold. According to the Bader analysis, the charges localized on the adsorbed Au and Au_2 are -0.08 e and -0.14 e, respectively, where e is an elementary charge.

However, the interaction of Au and Au_2 with the support becomes stronger when the h-BN surface contains V_B or V_N point defects. The strong adsorption on vacancy defects is accompanied by the large charge transfer to/from the gold particles. The calculated binding energies of Au and Au_2 to h-BN, V_B@h-BN and V_N@h-BN as well as Bader charges localized on the adsorbed gold are summarized in Table 1.

Table 1. Binding energies of Au and Au_2 to the support, and the Bader charges localized on the supported Au and Au_2.

Surface	$E_b(Au)$ **(eV)**	Q_{Au} **(|e|)**	$E_b(Au_2)$ **(eV)**	Q_{Au_2} **(|e|)**
h-BN	0.25	-0.08	0.77	-0.14
V_B@h-BN	3.72	0.70	3.24	0.57
V_N@h-BN	3.48	-0.39	3.07	-0.59

It is important to note that the charge of the adsorbed gold particles strongly depends on the type of vacancy defects, and can possess either negative or positive values. Figures 2 and 3 present the electron density differences $\Delta\rho(r)$ in Au/V_B@h-BN and Au/V_N@h-BN, respectively. Upper rows in Figures 2 and 3 present the electron density differences $\Delta\rho(r)$ projected on the plane passing through the adsorbed Au atom; while lower rows demonstrate $\Delta\rho(r)$ projected on the plane passing through three atoms N (B) atoms in the vicinity the V_B (V_N) vacancy defect on the h-BN surface. Blue and violet regions are electron poor, whereas red and pink are electron rich. It is seen from Figures 2 and 3 that V_N donates electrons to the adsorbed Au and Au_2; while V_B acts as an electron acceptor. Hence, it is possible to modify considerably the cluster's electron donor-acceptor capacity and its catalytic properties via the support design. To demonstrate this effect and to study the specific role played by the defected h-BN support in formation of the catalytic properties of gold we perform systematic investigation of adsorption and activation of O_2 on Au/h-BN and Au_2/h-BN systems.

Figure 2. The electron density difference in Au/V_B[@]h-BN induced by the interaction of Au with the boron vacancy V_B[@]h-BN, *i.e.*, ρ(Au/V_B[@]h-BN) − ρ(Au) − ρ(V_B[@]h-BN) and projected on the planes parallel to the h-BN surface. Plane passing through the adsorbed Au atom (upper row); plane passing through three N atoms nearby the boron vacancy V_B (lower row). Blue and violet regions correspond to the electron loss, whereas red and pink regions correspond to the excess of the electron charge.

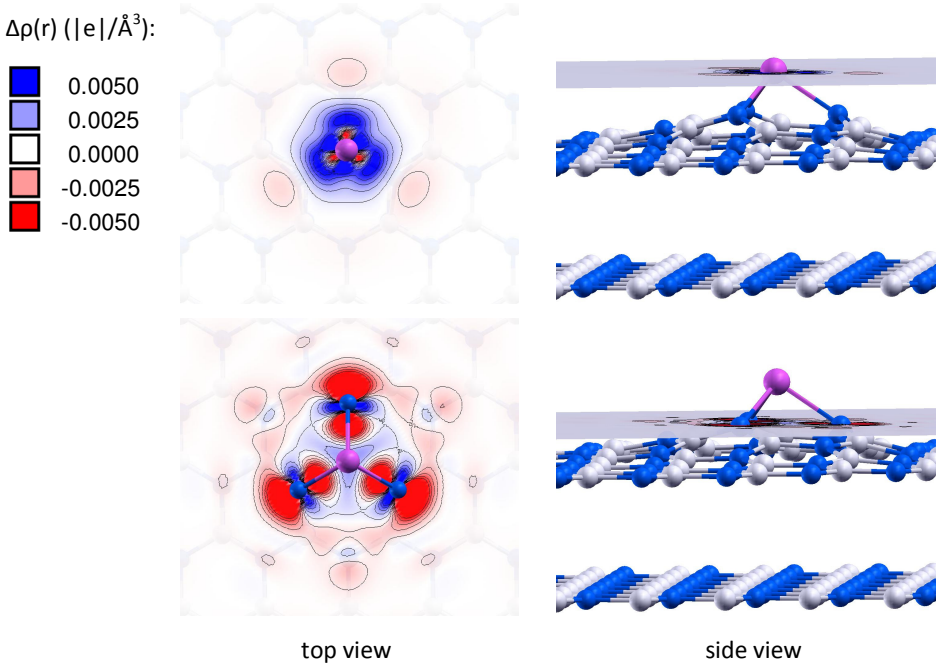

Figure 3. The same as in Figure 2, but for Au/V_N[@]h-BN.

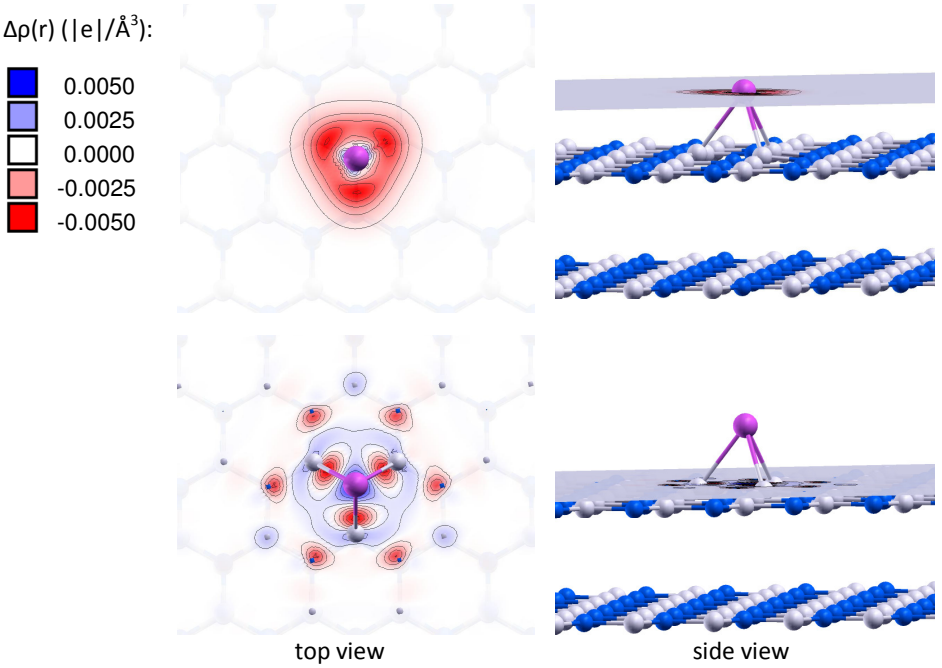

Adsorption of molecular oxygen on free gold clusters has been intensively investigated; see, e.g., References [10,29–31] and references therein. It was found that O_2 readily adsorbs and becomes catalytically activated on small neutral gold clusters with an odd number of atoms as well as on gold cluster anions. Such an ability of small gold clusters to bind and activate molecular oxygen has been explained by the transfer of unpaired valence electron from the cluster to the oxygen anti-bonding $2\pi^*$ orbital, see, e.g., References [10,29–31] and references therein. Our calculations demonstrate that O_2 adsorbs on the free Au and Au_2 with the binding energy of 0.49 eV and 0.48 eV, respectively. The O–O bond length enlarges from 1.24 Å (free O_2) to 1.27 Å and 1.26 Å, upon O_2 adsorption on gold monomer and dimer, respectively. Slight increase in the O–O bond length of the adsorbed O_2 demonstrates its catalytic activation.

Can the defected h-BN support modify the catalytic properties of gold? Our calculations demonstrate that O_2 readily adsorbs on Au and Au_2 trapped by the defected h-BN surface. Figure 4 presents optimized geometries of O_2 adsorbed on the free and supported Au and Au_2. It is seen from Figure 4 that oxygen molecule adsorbs on top of the Au atom trapped by the V_B[@]h-BN defect and bridges Au and B atoms in the case of adsorption on Au/V_N[@]h-BN. In the case of the supported gold dimer, O_2 bridges two gold atoms on Au_2/V_B[@]h-BN; while for the Au_2/V_N[@]h-BN system, O_2 bridges nearest to the surface Au atom, which is located on top of V_N and B atom on the surface. Therefore an interface between the supported gold cluster and the h-BN surface might play an important role in oxidation reactions on the supported gold clusters.

Figure 4. Optimized geometries of O_2 adsorbed on the free and supported Au and Au_2. The interatomic distances are given in Angstroms. Only part of the h-BN slab is shown.

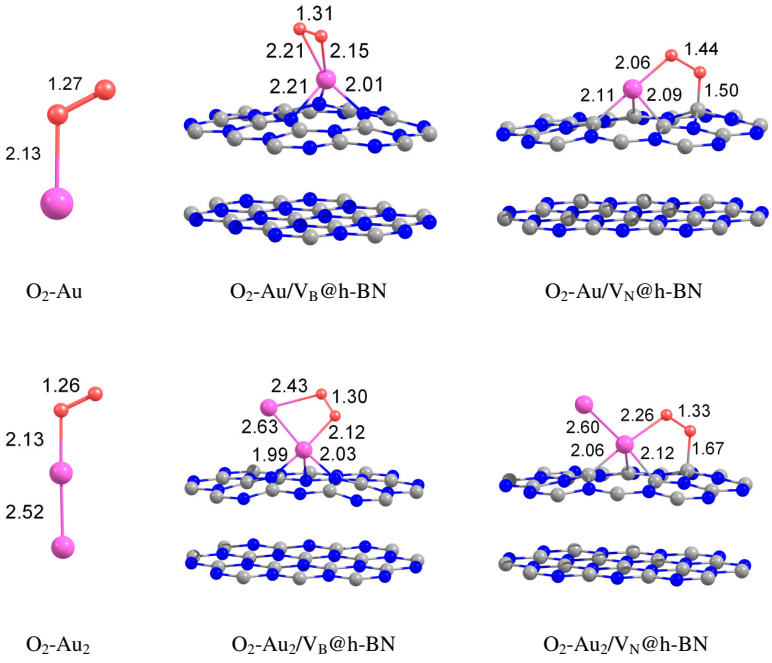

Interaction of Au and Au_2 with the support results in additional activation of the adsorbed O_2 and weakening of the O–O bond. This effect is especially strong for V_N vacancy defect, which acts as an electron donor for the supported Au and Au_2. Figure 4 demonstrates that the O–O bond length in adsorbed O_2 is enlarged similar to superoxide and peroxide states (the O–O bond distances in O_2^-

and O_2^{2-} are 1.33 Å and 1.49 Å [92], respectively). The results of our calculations demonstrate that interaction of Au and Au_2 with the defected h-BN surface can lead to a dramatic change in the catalytic activity of gold.

Table 2. Binding energies of O_2 to free and supported Au and Au_2; the O–O bond length, d_{O-O}, and the Bader charges localized on $Au_{1,2}$, O_2 and O_2-$Au_{1,2}$ calculated for free and supported Au and Au_2 with the adsorbed O_2.

Surface	$E_b(O_2)$**(eV)**	d_{O-O} **(Å)**	$Q_{Au_{1,2}}$ $(\|e\|)$	Q_{O_2} $(\|e\|)$	$Q_{O_2-Au_{1,2}}$ $(\|e\|)$
Au	0.49	1.27	0.19	−0.19	0.00
$Au/V_B{}^{@}$h-BN	0.90	1.31	0.98	−0.33	0.66
$Au/V_N{}^{@}$h-BN	1.10	1.44	−0.10	−1.31	−1.41
Au_2	0.48	1.26	0.15	−0.15	0.00

Table 2 presents the binding energies of O_2, $E_b(O_2)$, to the free and h-BN supported Au and Au_2. Interaction of Au and Au_2 with the h-BN support results in the considerable change in oxygen binding. Thus, O_2 adsorbs on $Au/V_B{}^{@}$h-BN and $Au/V_N{}^{@}$h-BN with binding energies of 0.90 eV and 1.10 eV, respectively. This is twice larger than the binding energy of O_2 to the free Au. The strong change in binding of O_2 to $Au/V_B{}^{@}$h-BN and $Au/V_N{}^{@}$h-BN can be explained by the large charge transfer between the corresponding point defects and the trapped Au atom. It is interesting that binding of O_2 to $Au_2/V_B{}^{@}$h-BN center is weaker if compared with free Au_2. However, adsorption of O_2 on $Au_2/V_N{}^{@}$h-BN is highly promoted. In the latter case O_2 bridges one of the gold atoms and the nearest boron atom on the surface, with binding energy of 1.30 eV. Thus, the oxygen binding to the supported gold particles considerably depends on the number of gold atoms and the type of the support. Activation and reactivity of the adsorbed O_2 are strongly affected by the charge transfer from the gold hybridized 5d6s orbitals to the anti-bonding $2\pi^*$ orbital of O_2. In the case of O_2 adsorption on free Au, the Bader charge localized on O_2 is -0.19 e. The charge transfer from Au to O_2 is responsible for the catalytic activation of the adsorbed O_2 and weakening of the O–O bond. Interaction of Au with the defected h-BN support results in the drastic increase in charge transfer to the adsorbed O_2. That means that the interaction of Au and Au_2 with the defected h-BN support considerably promotes the charge transfer from the gold to O_2. Such an effect becomes very clear for O_2 adsorbed on the $Au/V_B{}^{@}$h-BN center. As we have discussed above, the B vacancy acts as an electron acceptor. Thus, Au trapped by the $V_B{}^{@}$h-BN defect possesses a positive charge. It is well known that free gold cluster cations are inert toward molecular oxygen. However, our calculations demonstrate that O_2 readily adsorbs and becomes highly activated on the positively charged $Au/V_B{}^{@}$h-BN center. Interaction with the $V_B{}^{@}$h-BN support promotes additional charge transfer (in comparison with O_2 adsorbed on free Au) from the gold to the adsorbed O_2, even if the adsorbed Au has a positive charge. This effect is rather similar to that of promotion of oxygen activation by the small gold clusters with coadsorbed hydrogen [27] or ethylene [11] molecules. In the case of O_2 adsorption on the $Au/V_N{}^{@}$h-BN center, gold atom trapped by the N vacancy has a negative charge. That promotes charge transfer to the adsorbed O_2. However, in contrast to the case of the $Au/V_B{}^{@}$h-BN adsorption

center, the additional charge transfer to the oxygen adsorbed on $Au/V_N{}^{@}$h-BN occurs mainly due to the charge transfer from the support.

It is seen from Table 2 that adsorption of O_2 on $Au_2/V_B{}^{@}$h-BN is accompanied by the additional charge transfer from Au_2, while the total charge transfer from the $V_B{}^{@}$h-BN support to the Au_2 and O_2-Au_2 adsorbates remains unchanged. Hence, interaction of Au_2 with the $V_B{}^{@}$h-BN defect promotes charge transfer from the gold to the oxygen. However, in the case of O_2 adsorption on $Au_2/V_N{}^{@}$h-BN center an additional charge transfer to O_2 occurs mainly due to the charge transfer from the $V_N{}^{@}$h-BN center, but not from the gold dimer. In both cases charge transfer to O_2 is accompanied by its strong activation.

Thus, we found that strong adsorption of Au and Au_2 on the surface defects is accompanied by the charge transfer to/from the adsorbate. The value and the sign of the charge accumulated on the adsorbate depend on the adsorption sites. Thus, V_N donates electrons to the adsorbed Au and Au_2; while V_B acts as an electron acceptor. The excess of the positive or negative charge on the supported gold clusters can considerably promote their catalytic properties and enhance activation of the adsorbed O_2.

3.2. Adsorption and Dissociation of H_2 on $Au_n/TiO_2(110)$. Interface Effects

Let us consider catalytic activity of gold clusters supported on the active surface of rutile $TiO_2(110)$. The $TiO_2(110)$ surface contains oxygen and titanium atoms with different coordination. The fivefold coordinated Ti atoms are undercoordinated relatively to the bulk sixfold coordinated Ti, as it is shown in Figure 5. The O atoms raised above the plane of Ti atoms are twofold coordinated. These atoms are called bridge-site O. The oxygen atoms lying in the plane of Ti atoms are threefold coordinated. Relaxation of the $TiO_2(110)$ surface results in a surface rumpling, as it is shown in Figure 5. The undercoordinated Ti and O atoms are moving inward by 0.10 Å, decreasing the distance with subsurface atoms. The sixfold coordinated Ti atoms and threefold coordinated O atoms are moving outward by 0.1 Å and 0.2 Å, respectively. The similar puckered structure of the rutile (110) surface has been reported in References [93,94].

Figure 5. Side view of the $TiO_2(110)$ p (2×5) slab. The bridge-site twofold coordinated O(2) atom, threefold coordinated O(3) atom, five- and six-fold coordinated Ti(5) and Ti(6) atoms are marked, respectively. Relaxation of the $TiO_2(110)$ surface results in a surface rumpling.

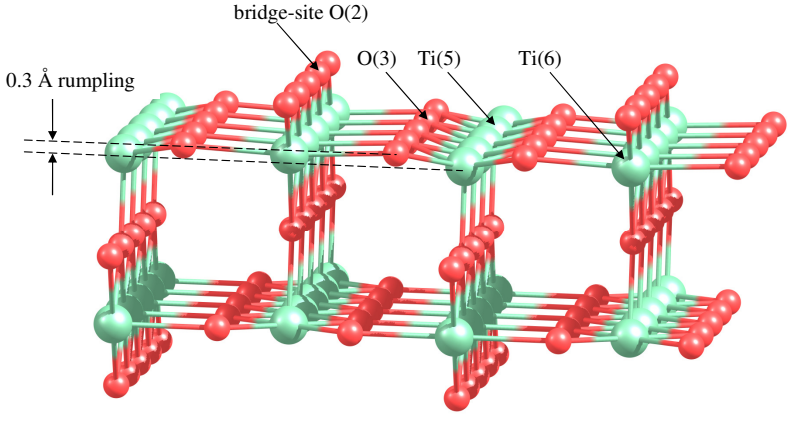

Our calculations demonstrate that H_2 can be adsorbed on the pure, defect-free TiO_2(110) surface, even in the absence of the gold particle. The most stable geometries calculated for the molecular and dissociative adsorption of H_2 on the pure rutile TiO_2(110) surface are presented in Figure 6. It is seen that H_2 preferably adsorbs on top of the Ti(5) atom with the binding energy of 0.14 eV. The H–H bond length of 0.78 Å is slightly increased in comparison with the free H_2. The dissociative state of H_2 on TiO_2(110) corresponds to the situation when both H atoms form the OH group with the low coordinated O(2) bridge atoms on the rutile surface. The binding energy of the dissociated configuration of H_2 is 1.50 eV; however, the distance between two rows of O(2) atoms on TiO_2(110) is 6.50 Å, which is too large to promote dissociation of the H_2 adsorbed on top of Ti(5) atom. In this case H_2 would dissociate in the vicinity of the adsorption center as a first step, followed by adsorption of H atoms on O(2). This process requires to overcome a dissociation barrier of ∼4.3 eV which is much higher than the energy of the molecular adsorption. In this situation H_2 would desorb from the surface and fly away rather than dissociate. Therefore, to promote H_2 dissociation on TiO_2(110), it is necessary to have adsorption centers on the rutile surface in the vicinity of low coordinated O(2) atoms. Supported gold clusters can serve as a source of such centers.

Figure 6. Optimized geometries for molecular (left) and dissociative (right) adsorption of H_2 on the pure rutile TiO_2(110) surface.

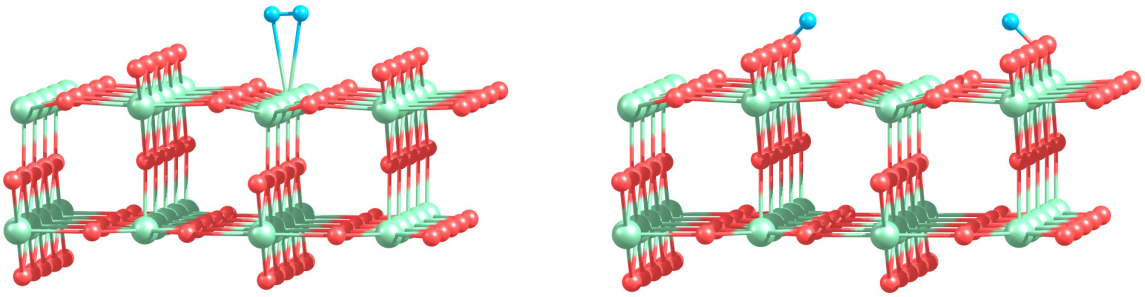

In the present work we consider adsorption of H_2 on the most stable isomers of free and supported gold clusters Au_n consisting of $n = 1$, 2, 8 and 20 atoms. Figure 7 presents the optimized geometries of H_2-Au_n systems in the case of molecular and dissociative adsorption of H_2 on free Au_n clusters. In order to obtain the most stable configuration of H_2 adsorbed on Au_n, we have created a large number of starting geometries by adding H_2 molecule in different positions (up to 30) on the surface of the considered clusters. The starting structures have been optimized further without any geometric constraints. We have successfully used a similar approach to find the optimized geometries of O_2 and C_2H_4 molecules adsorbed on small neutral, anionic and cationic gold clusters [10,11,37,95]. The binding energies for molecular, E_b^{mol}, and dissociative, E_b^{dis}, adsorption of H_2 on free Au_n as well as the H–H bond length r_{H-H}^{mol} in H_2 adsorbed molecularly are summarized in Table 3.

Results of our calculations demonstrate that H_2 binds weakly to Au as a molecule, with E_b^{mol} = 0.13 eV. Dissociation of H_2 on Au is not favorable energetically. The H–H bond length in H_2 adsorbed on Au is slightly enlarged in comparison with the free H_2. Adsorption of H_2 on Au_2 is relatively strong, with the binding energy equal to 0.59 eV both for the molecular and the dissociative adsorption. Table 3 demonstrates that the H–H bond length increases to 0.845 Å in H_2-Au_2, indicating

that H_2 is highly activated. With the further increase in cluster size the binding energy calculated for molecular adsorption of H_2 decreases to 0.26 eV for Au_8 and 0.09 eV both for Au_{20}. On the other hand, the dissociative adsorption of H_2 becomes energetically favorable both for Au_8 and Au_{20}.

Figure 7. Optimized geometries of H_2-Au_n clusters in the case of molecular (left) and dissociative (right) adsorption of H_2.

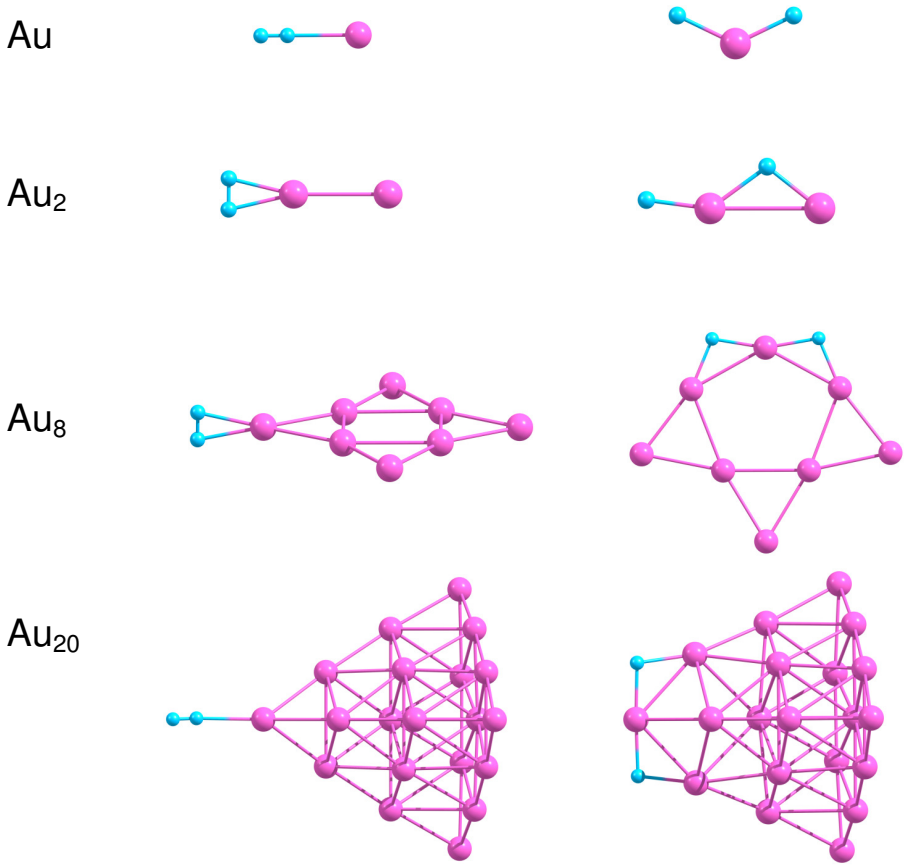

Table 3. Binding energies for molecular, E_b^{mol}, and dissociative, E_b^{dis}, adsorption of H_2 on the most stable free Au_n clusters and the H−H bond length, $r_{\mathrm{H-H}}^{mol}$, in the case of molecular adsorption of H_2.

Cluster	$r_{\mathrm{H-H}}^{mol}$ **(Å)**	E_b^{mol} **(eV)**	E_b^{dis} **(eV)**
Au	0.780	0.13	0.04
Au_2	0.845	0.59	0.59
Au_8	0.806	0.26	0.68
Au_{20}	0.768	0.09	0.14

One of the factors that influence H_2 dissociation is coordination of Au atoms interacting with hydrogen and flexibility of cluster structure, as was discussed in [96]. It is seen from Figure 7 that H_2 dissociates at the low coordinated corner Au atom with formation of the slightly bent H–Au–H bond.

Note, that the Au–Au bond length in Au_2 does not change noticeably upon molecular adsorption of H_2; but increases up to 2.753 Å for dissociative adsorption. In the case of Au_8 and Au_{20} dissociation of H_2 on the cluster surface is accompanied by the structural (at least local) transformations, although Au_{20} demonstrates rather strong structural stability, due to the "magic" nature of this cluster.

How does the interaction with the support influence the reactivity of gold clusters? In the present work we perform a systematic theoretical study of the structure and energetics of H_2 adsorbed on Au_1, Au_2, Au_8 Au_{20} clusters supported on the rutile $TiO_2(110)$ surface. The analysis of the energetics of H_2 adsorption on the supported gold clusters provides deep insights into the nature of bonding and dissociation of the H_2 molecule and reveals the details of the reaction mechanism. Figure 8 shows the most stable geometries of H_2 adsorbed on the supported gold clusters. The binding energies calculated for molecular, E_b^{mol}, and dissociative, E_b^{dis}, adsorption of H_2 on Au_n/TiO_2, and the H−H bond length, r_{H-H}^{mol}, in the case of molecular adsorption of H_2 are summarized in Table 4.

Figure 8. The most stable geometries of H_2 adsorbed on Au_n/TiO_2 clusters in the case of molecular (left) and dissociative (right) adsorption of H_2.

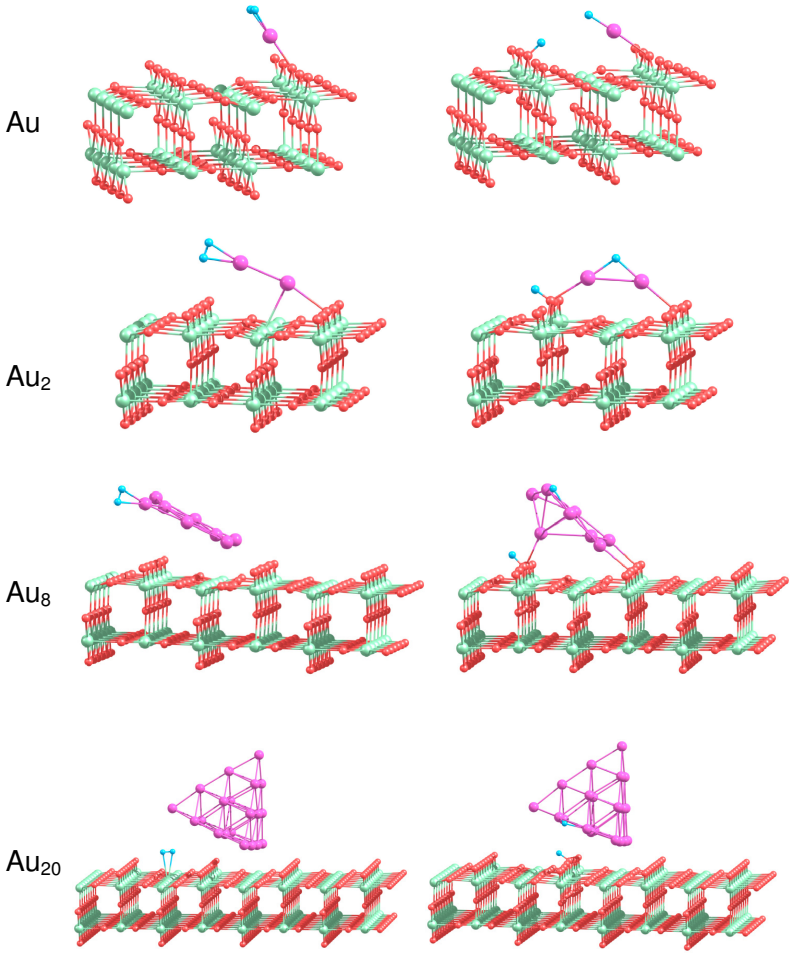

Table 4. Binding energy calculated for molecular, E_b^{mol}, and dissociative, E_b^{dis}, adsorption of H_2 on Au_n/TiO_2, and the H−H bond length, r_{H-H}^{mol}, in the case of molecular adsorption of H_2.

Cluster	r_{H-H}^{mol} (Å)	E_b^{mol} (eV)	E_b^{dis} (eV)
Au/TiO_2	0.906	1.15	2.06
Au_2/TiO_2	0.821	0.37	1.55
Au_8/TiO_2	0.792	0.24	1.55
Au_{20}/TiO_2	0.795	0.17	0.83

It is seen from Table 4 that H_2 adsorbs molecularly on Au/TiO_2 with a binding energy of 1.15 eV, which is considerably larger than the corresponding energy calculated for H_2 adsorbed on free Au atom. The adsorbed H_2 is highly activated, with the H−H bond length r_{H-H}^{mol} = 0.906 Å. As a result of H_2 adsorption, the supported Au atom shifts slightly towards the row of the low coordinated O(2) bridge atoms. In the previous section we demonstrated that H_2 dissociation is not favorable on the free Au atom. However, in the case of the supported Au atom, dissociation of H_2 can occur with formation of the OH group with the O(2) atom located either in the nearest to Au row of O(2) or in the next row of O(2), as is shown in Figure 8. In the latter case the calculated binding energy E_b^{dis} = 2.06 eV is higher, not only if compared with the binding energy for molecular adsorption of H_2 on $Au/TiO_2(110)$, but also if compared with the binding energy of the dissociated state of H_2 on the pure $TiO_2(110)$ surface. Thus, we can conclude, from the energetic point of view, that the $TiO_2(110)$ support considerably promotes H_2 dissociation on Au atom.

We found that molecular H_2 binds to the supported Au_2 in a similar way as for the free Au_2. However, the binding energy calculated for the molecular adsorption of H_2 on Au_2/TiO_2 is lower than the corresponding energy obtained for free Au_2. The dissociated hydrogen atom can migrate to the row of O(3) atoms, or to the row of O(2) bridge atoms on the rutile surface, forming OH bonds. The interaction of Au_2 with the support results in the energetic promotion of H_2 dissociation on the supported Au_2.

The optimized geometries of H_2 in the case of its molecular adsorption on the supported Au_8 cluster similar to those obtained for the corresponding free Au_8. However, the dissociative adsorption of H_2 on Au_8 results in the considerable rearrangement of the cluster structure. The dissociative configuration of H_2 on the supported Au_8 is promoted energetically. Migration of H on the low coordinated O(2) atom results in formation of the OH bond and considerable increase in binding energies calculated for H_2 adsorbed dissociatively.

The Au_{20} clusters supported on $TiO_2(110)$ are the largest systems studied in the present work. It was shown above that the hydrogen molecule binds weakly to the free Au_{20} clusters. We have found that, in the case of the supported Au_{20}, the hydrogen molecule adsorbs on top of the Ti(5) atoms on the rutile surface in the vicinity of Au_{20}, rather than directly on the Au_{20} clusters. After H_2 dissociation in the vicinity of Au_{20}/TiO_2 one of the H atoms binds to the edge of Au_{20} that are oriented perpendicularly to the rows of O(2) surface atoms, while another H forms the OH bond with the O(2) atom on the rutile surface. However, this configuration is not stable in comparison with the situation when both of H atoms

form OH surface group. Therefore, H atom on the edge of the supported Au_{20} cluster will further migrate towards the low coordinated O(2) atoms on the rutile surface.

Our calculations demonstrate that combination (interplay) of several factors such as geometric structure, presence of the low coordinated oxygen atoms in the vicinity of the cluster-surface interface, *etc*., are important for H_2 dissociation. What is the role of the charge transfer from the gold cluster to hydrogen in H_2 dissociation? As it was discussed in previous section, the charge transfer from the gold to the antibonding orbital of O_2 is responsible for the catalytic activation of O_2. However, in the case of H_2 dissociation the analysis of the Bader charges [79,80] demonstrate that there is no considerable charge transfer between the adsorbed hydrogen and the gold clusters (free or supported). Thus, the largest charge transfer occurs for H_2 adsorbed molecularly on Au/TiO_2. In this case the calculated Bader charge localized on H_2 is $+0.11$ e, where e is the elementary charge. Although such a charge transfer is relatively small, it might be responsible for the strong enlargement of the H−H bond length in H_2-Au/TiO_2 up to 0.906 Å. In most cases of molecular adsorption of hydrogen, the adsorbed molecule possesses some small positive charge. However, after dissociation, the hydrogen atoms can get an excess of negative charge. Depending on the geometric configuration, either both of the hydrogen atoms possess some small negative charge, or one H is charged negatively, while another H is charged positively. Thus, for example the H−H bond cleavage on the unsupported Au_2 can be considered as heterolytic—one H possesses negative charge of -0.11 e, while another H possesses very small positive charge of $+0.01$ e. In this case the gold dimer becomes positively charged upon H_2 dissociation with the net charge of $+0.1$ e. On the other hand, formation of the OH group with the bridge O(2) atom on the rutile surface is accompanied by the large charge transfer from H atom to O(2), resulting in a Bader net charge of H in OH equal to $+0.75$ e. Another H on Au cluster remains negatively charged. Note that formation of the hydrogen anions on the gold surface can influence probability of further hydrogenation reactions catalyzed by the supported gold clusters.

We can conclude that the catalytic activity of gold nanoparticles for O_2 dissociation would depend on the electronic structure and the size of the nanoparticles; however in the case of H_2 dissociation it will be proportional to the number of gold atoms located in the vicinity of the low coordinated O(2) atoms at the nanoparticle-surface interface.

4. Conclusions

The present theoretical study demonstrates the support effects are very important in the gold nanocatalysis. Even "inert" h-BN support, if it contains vacancy defects, can promote the catalytic properties of gold clusters in oxidation reaction by O_2. It is demonstrated that Au and Au_2 interact weakly with the regular defect-free h-BN surface; however they can be trapped effectively by N or B vacancy defects in h-BN. Strong adsorption on the surface defects is accompanied by the charge transfer to/from the adsorbate. The value and the sign of the charge accumulated on the adsorbate depend on the adsorption sites. Thus, V_N donates electrons to the adsorbed Au and Au_2, while V_B acts as an electron acceptor. The excess of the positive or negative charge on the supported gold clusters can considerably promote their catalytic properties and enhance activation of the adsorbed O_2. Our finding leads to a very important conclusion that gold clusters supported on the defected h-BN surface can not be considered as pseudo-free clusters. The support effects have to be taken into account.

We also demonstrate that the "active" rutile TiO_2(110) support energetically promotes H_2 dissociation on gold clusters. For this reaction the conventional charge transfer mechanism does not play an important role. However, adsorption of H_2 on Au_n and Au_n/TiO_2(110) (n = 1, 2, 8, 20) strongly depends on cluster size, geometric structure, flexibility and interaction with the support material. We demonstrate that the formation of the OH group near the supported gold cluster is an important condition for H_2 dissociation. We have shown that the active sites towards H_2 dissociation on the supported Au_n are located at corners and edges of the gold cluster in the vicinity of the low coordinated oxygen atoms on TiO_2(110). Therefore catalytic activity of a gold nanoparticle supported on the rutile TiO_2(110) surface is proportional to the length of the perimeter interface between the nanoparticle and the support, in accordance with the recent experimental findings [38].

Acknowledgements

This work was supported by the Global COE Program (Project No. B01: Catalysis as the Basis for Innovation in Materials Science) from the Ministry of Education, Culture, Sports, Science and Technology, Japan; the Grant-in-Aid for the Project on Strategic Utilization of Elements; the JSPS Grant-in-Aid for Scientific Research C; and the Collaborative Research Program 2011, Information Initiative Center, Hokkaido University, Sapporo, Japan. The computations were partly performed using the Research Center for Computational Science, Okazaki, Japan.

References

1. Haruta, M.; Kobayashi, T.; Sano, H.; Yamada, N. Novel gold catalysts for the oxidation of carbon monoxide at a temperature far below 0 °C. *Chem. Lett.* **1987**, *16*, 405–408.
2. Haruta, M. When gold is not noble: Catalysis by nanoparticles. *Chem. Rec.* **2003**, *3*, 75–87.
3. Thompson, D.T. Using gold nanoparticles for catalysis. *Nanotoday* **2007**, *2*, 40–43.
4. *Nanocatalysis*; Heiz, U., Landman, U., Eds.; Springer: Berlin, Heidelberg, Germany, 2007.
5. Haruta, M. Size- and support-dependency in the catalysis of gold. *Catal. Today* **1997**, *36*, 153–166.
6. Turner, M.; Golovko, V.B.; Vaughan, O.P.H.; Abdulkin, P.; Berenguer-Murcia, A.; Tikhov, M.S.; Johnson, B.F.G.; Lambert, R.M. Selective oxidation with dioxygen by gold nanoparticle catalysts derived from 55-atom clusters. *Nature* **2008**, *454*, 981–984.
7. Hughes, M.D.; Xu, Y.J.; Jenkins, P.; McMorn, P.; Landon, P.; Enache, D.I.; Carley, A.F.; Attard, G.A.; Hutchings, G.J.; King, F.; Stitt, E.H.; Johnston, P.; Griffin, K.; Kiely, C.J. Tunable gold catalysts for selective hydrocarbon oxidation under mild conditions. *Nature* **2005**, *437*, 1132–1135.
8. Tsunoyama, H.; Sakurai, H.; Negishi, Y.; Tsukuda, T. Size-specific catalytic activity of polymer-stabilized gold nanoclusters for aerobic alcohol oxidation in water. *J. Am. Chem. Soc.* **2005**, *127*, 9374–9375.
9. Landon, P.; Collier, P.J.; Papworth, A.J.; Kiely, C.J.; Hutchings, G. Direct formation of hydrogen peroxide from H_2/O_2 using a gold catalyst. *Chem. Commun.* **2002**, 2058–2059; doi:10.1039/B205248M.

10. Lyalin, A.; Taketsugu, T. Cooperative adsorption of O_2 and C_2H_4 on small gold clusters. *J. Phys. Chem. C* **2009**, *113*, 12930–12934.
11. Lyalin, A.; Taketsugu, T. Reactant-promoted oxygen dissociation on gold clusters. *J. Phys. Chem. Lett.* **2010**, *1*, 1752–1757.
12. Jia, J.; Haraki, K.; Kondo, J.N.; Domen, K.; Tamaru, K. Selective hydrogenation of acetylene over Au/Al_2O_3 catalyst. *J. Phys. Chem. B* **2000**, *104*, 11153–11156.
13. Choudhary, T.V.; Sivadinarayana, C.; Datye, A.K.; Kumar, D.; Goodman, D.W. Acetylene hydrogenation on Au-based catalysts. *Catal. Lett.* **2003**, *86*, 1–8.
14. Bailie, J.E.; Hutchings, G.J. Promotion by sulfur of gold catalysts for crotyl alcohol formation from crotonaldehyde hydrogenation. *Chem. Commun.* **1999**, 2151–2152; doi:10.1039/A906538E.
15. Schimpf, S.; Martin Lucas, M.; Mohra, C.; Rodemerck, U.; Brückner, A.; Radnik, J.; Hofmeister, H.; Claus, P. Supported gold nanoparticles: In-depth catalyst characterization and application in hydrogenation and oxidation reactions. *Catal. Today* **2002**, *72*, 63–78.
16. Okumura, M.; Akita, T.; Haruta, M. Hydrogenation of 1,3-butadiene and of crotonaldehyde over highly dispersed au catalysts. *Catal. Today* **2002**, *74*, 265–269.
17. Mohr, C.; Hofmeister, H.; Radnik, J.; Claus, P. Identification of active sites in gold-catalyzed hydrogenation of acrolein. *J. Am. Chem. Soc.* **2003**, *125*, 1905–1911.
18. Zanella, R.; Louis, C.; Giorgio, S.; Touroude, R. Crotonaldehyde hydrogenation by gold supported on TiO_2: Structure sensitivity and mechanism. *J. Catal.* **2004**, *223*, 328–339.
19. Claus, P. Heterogeneously catalysed hydrogenation using gold catalysts. *Appl. Catal. A Gen.* **2005**, *291*, 222–229.
20. Zhu, Y.; Qian, H.; Drake, B.A.; Jin, R. Atomically precise $Au_{25}(SR)_{18}$ nanoparticles as catalysts for the selective hydrogenation of α,β-unsaturated ketones and aldehydes. *Angew. Chem. Int. Ed.* **2010**, *49*, 1295–1298.
21. Zhu, Y.; Wu, Z.; Gayathri, C.; Qian, H.; Gil, R.R.; Jin, R. Exploring stereoselectivity of Au_{25} nanoparticle catalyst for hydrogenation of cyclic ketone. *J. Catal.* **2010**, *271*, 155–160.
22. Herzing, A.A.; Kiely, C.J.; Carley, A.F.; Landon, P.; Hutchings, G.J. Identification of active gold nanoclusters on iron oxide supports for CO oxidation. *Science* **2008**, *321*, 1331–1335.
23. Rodríguez-Vázquez, M.J.; Blanco, M.C.; Lourido, R.; Vázquez-Vázquez, C.; Pastor, E.; Planes, G.A.; Rivas, J.; López-Quintela, M.A. Synthesis of atomic gold clusters with strong electrocatalytic activities. *Langmuir* **2008**, *24*, 12690–12694.
24. Heiz, U.; Sanchez, A.; Abbet, S.; Schneider, W.D. Catalytic oxidation of carbon monoxide on monodispersed platinum clusters: Each atom counts. *J. Am. Chem. Soc.* **1999**, *121*, 3214–3217.
25. Bonačić-Koutecký, V.; Mitrić, R.; Bürgel, C.; Bchäfer-Bung, B. Cluster properties in the regime in which each atom counts. *Comput. Mater. Sci.* **2006**, *35*, 151–157.
26. Hvolbæk, B.; Janssens, T.V.W.; Clausen, B.S.; Falsig, H.; Christensen, C.H.; Nørskov, J.K. Catalytic activity of Au nanoparticles. *Nanotoday* **2007**, *2*, 14–18.
27. Lang, S.M.; Bernhardt, T.M.; Barnett, R.N.; Yoon, B.; Landman, U. Hydrogen-promoted oxygen activation by free gold cluster cations. *J. Am. Chem. Soc.* **2009**, *131*, 8939–8951.

28. Bürgel, C.; Reilly, N.M.; Johnson, G.E.; Mitrić, R.; Kimble, M.L.; Castleman, A.W., Jr.; Bonačić-Koutecký, V. Influence of charge state on the mechanism of CO oxidation on gold clusters. *J. Am. Chem. Soc.* **2008**, *130*, 1694–1698.
29. Coquet, R.; Howard, K.L.; Willock, D.J. Theory and simulation in heterogeneous gold catalysis. *Chem. Soc. Rev.* **2008**, *37*, 2046–2076.
30. Ding, X.; Li, Z.; Yang, J.; Hou, J.G.; Zhu, Q. Adsorption energies of molecular oxygen on Au clusters. *J. Chem. Phys.* **2004**, *120*, 9594–9600.
31. Fernández, E.; Ordejón, P.; Balbás, L.C. Theoretical study of O_2 and CO adsorption on Au_n clusters ($n = 5$–10). *Chem. Phys. Lett.* **2005**, *408*, 252–257.
32. Häkkinen, H.; Landman, U. Gas-phase catalytic oxidation of CO by Au_2^-. *J. Am. Chem. Soc.* **2001**, *123*, 9704–9705.
33. Yoon, B.; Häkkinen, H.; Landman, U. Interaction of O_2 with gold clusters: Molecular and dissociative adsorption. *J. Phys. Chem. A* **2003**, *107*, 4066–4071.
34. Socaciu, L.D.; Hagen, J.; Bernhardt, T.M.; Wöste, L.; Heiz, U.; Häkkinen, H.; Landman, U. Catalytic CO oxidation by free Au_2^-: Experiment and theory. *J. Am. Chem. Soc.* **2003**, *125*, 10437–10445.
35. Häkkinen, H.; Abbet, S.; Sanchez, A.; Heiz, U.; Landman, U. Structural, electronic, and impurity-doping effects in nanoscale chemistry: Supported gold nanoclusters. *Angew. Chem. Int. Ed.* **2003**, *42*, 1297–1300.
36. Hutchings, G.J.; Hall, M.S.; Carley, A.F.; Landon, P.; Solsona, B.E.; Kiely, C.J.; Herzing, A.; Makkee, M.; Moulijn, J.A.; Overweg, A.; Fierro-Gonzalez, J.C.; Guzman, J.; Gates, B.C. Role of gold cations in the oxidation of carbon monoxide catalyzed by iron oxide-supported gold. *J. Catal.* **2006**, *242*, 71–81.
37. Lyalin, A.; Taketsugu, T. Adsorption of ethylene on neutral, anionic, and cationic gold clusters. *J. Phys. Chem. C* **2010**, *114*, 2484–2493.
38. Fujitani, T.; Nakamura, I.; Akita, T.; Okumura, M.; Haruta, M. Hydrogen dissociation by gold clusters. *Angew. Chem. Int. Ed.* **2009**, *48*, 9515–9518.
39. Okumura, M.; Tsubota, S.; Haruta, M. Preparation of supported gold catalysts by gas-phase grafting of gold acethylacetonate for low-temperature oxidation of CO and of H_2. *J. Mol. Catal. A Chem.* **2003**, *199*, 73–84.
40. Sanchez, A.; Abbet, S.; Heiz, U.; Schneider, W.D.; Hakkinen, H.; Barnett, R.N.; Landman, U. When gold is not noble: Nanoscale gold catalysts. *J. Phys. Chem. A* **1999**, *103*, 9573–9578.
41. Yoon, B.; Häkkinen, H.; Landman, U.; Wörz, A.S.; Antonietti, J.M.; Abbet, S.; Judai, K.; Heiz, U. Charging effects on bonding and catalyzed oxidation of CO on Au_8 clusters on MgO. *Science* **2005**, *307*, 403–407.
42. Zhang, C.; Yoon, B.; Landman, U. Predicted oxidation of CO catalyzed by Au nanoclusters on a thin defect-free MgO film supported on a Mo(100) surface. *J. Am. Chem. Soc.* **2007**, *129*, 2228–2229.
43. Sterrer, M.; Risse, T.; Pozzoni, U.; Giordano, L.; Heyde, M.; Rust, H.; Pacchioni, G.; Freund, H. Control of the charge state of metal atoms on thin MgO films. *Phys. Rev. Lett.* **2007**, *98*, 096107:1–096107:4.

44. Frondelius, P.; Häkkinen, H.; Honkala, K. Adsorption of gold clusters on metal-supported MgO: Correlation to electron affinity of gold. *Phys. Rev. B* **2007**, *76*, 073406:1–073406:4.
45. Honkala, K.; Häkkinen, H. Au adsorption on regular and defected thin MgO(100) films supported by Mo. *J. Phys. Chem. C* **2007**, *111*, 4319–4327.
46. Harding, C.; Habibpour, V.; Kunz, S.; Farnbacher, A.N.S.; Heiz, U.; Yoon, B.; Landman, U. Control and manipulation of gold nanocatalysis: Effects of metal oxide support thickness and composition. *J. Am. Chem. Soc.* **2009**, *131*, 538–548.
47. Arenal, R.; Stéphan, O.; Kociak, M.; Taverna, D.; Loiseau, A.; Colliex, C. Electron energy loss spectroscopy measurement of the optical gaps on individual boron nitride single-walled and multiwalled nanotubes. *Phys. Rev. Lett.* **2005**, *95*, 127601:1–127601:4.
48. Golberg, D.; Bando, Y.; Huang, Y.; Terao, T.; Mitome, M.; Tang, C.; Zhi, C. Boron nitride nanotubes and nanosheets. *ACS Nano* **2010**, *4*, 2979–2993.
49. Green, I.X.; Tang, W.; Neurock, M.; Yates, J.T. Low-temperature catalytic H_2 oxidation over Au nanoparticle/TiO_2 dual perimeter sites. *Angew. Chem. Int. Ed.* **2011**, *50*, 10186–10189.
50. Boronat, M.; Illas, F.; Corma, A. Active sites for H_2 adsorption and activation in Au/TiO_2 and the role of the support. *J. Phys. Chem. A* **2009**, *113*, 3750–3757.
51. Florez, E.; Gomez, T.; Liu, P.; Rodríguez, J.A.; Illas, F. Hydrogenation reactions on Au/TiC(001): Effects od Au-C interactions on the dissociation of H_2. *ChemCatChem* **2010**, *2*, 1219–1222.
52. Lyalin, A.; Taketsugu, T. A computational investigation of H_2 adsorption and dissociation on Au nanoparticles supported on TiO_2 surface. *Faraday Discuss.* **2011**, *152*, 185–201.
53. Wu, Z.; Cohen, R.E. More accurate generalized gradient approximation for solids. *Phys. Rev. B* **2006**, *73*, 235116:1–235116:6.
54. Perdew, J.P.; Burke, K.; Ernzerhof, M. Generalized gradient approximation made simple. *Phys. Rev. Lett.* **1996**, *77*, 3865–3868.
55. Tran, F.; Laskowski, R.; Blaha, P.; Schwarz, K. Performance on molecules, surfaces, and solids of the Wu-Cohen GGA exchange-correlation energy functional. *Phys. Rev. B* **2007**, *75*, 115131:1–115131:14.
56. Artacho, E.; Sánchez-Portal, D.; Ordejón, P.; García, A.; Soler, J.M. Linear-scaling ab-initio calculations for large and complex systems. *Phys. Status Solidi B* **1999**, *215*, 809–817.
57. Junquera, J.; Paz, O.; Sánchez-Portal, D.; Artacho, E. Numerical atomic orbitals for linear-scaling calculations. *Phys. Rev. B* **2001**, *64*, 235111:1–235111:9.
58. Nelder, J.A.; Mead, R. A simplex method for function minimization. *Comput. J.* **1965**, *7*, 308–313.
59. Troullier, N.; Martins, J.L. Efficient pseudopotentials for plane-wave calculations. *Phys. Rev. B* **1991**, *43*, 1993–2006.
60. Kleinman, L.; Bylander, D.M. Efficacious form for model pseudopotentials. *Phys. Rev. Lett.* **1982**, *48*, 1425–1428.
61. Monkhorst, H.J.; Pack, J.D. Special points for Brillouin-zone integrations. *Phys. Rev. B* **1976**, *13*, 5188–5192.
62. Yoo, C.S.; Akella, J.; Cynn, H.; Nicol, M. Direct elementary reactions of boron and nitrogen at high pressures and temperatures. *Phys. Rev. B* **1997**, *56*, 140–146.

63. Burdett, J.K.; Hughbanks, T.; Miller, G.J.; Richardson, J.W., Jr.; Smith, J.V. Structural-electronic relationships in inorganic solids: Powder neutron diffraction studies of the rutile and anatase polymorphs of titanium dioxide at 15 and 295 K. *J. Am. Chem. Soc.* **1987**, *109*, 3639–3646.
64. Muscat, J.; Swamy, V.; Harrison, N.M. First-principles calculations of the phase stability of TiO_2. *Phys. Rev. B* **2002**, *65*, 224112:1–224112:15.
65. Solov'yov, I.A.; Solov'yov, A.V.; Greiner, W.; Koshelev, A.; Shutovich, A. Cluster growing process and a sequence of magic numbers. *Phys. Rev. Lett.* **2003**, *90*, 053401:1–053401:4.
66. Lyalin, A.; Solov'yov, I.A.; Solov'yov, A.V.; Greiner, W. Evolution of the electronic and ionic structure of Mg clusters with increase in cluster size. *Phys. Rev. A* **2003**, *67*, 063203:1–063203:13.
67. Lyalin, A.; Solov'yov, A.V.; Greiner, W. Structure and magnetism of lanthanum clusters. *Phys. Rev. A* **2006**, *74*, 043201:1–043201:10.
68. Lyalin, A.; Solov'yov, I.A.; Greiner, W. Interplay of electronic and geometry shell effects in properties of neutral and charged Sr clusters. *Phys. Rev. A* **2007**, *75*, 053201:1–053201:13.
69. Ohno, K.; Maeda, S. A scaled hypersphere search method for the topography of reaction pathways on the potential energy surface. *Chem. Phys. Lett.* **2004**, *384*, 277–282.
70. Maeda, S.; Ohno, K. Global mapping of equilibrium and transition structures on potential energy surfaces by the scaled hypersphere search method: Applications to ab initio surfaces of formaldehyde and propyne molecules. *J. Phys. Chem. A* **2005**, *109*, 5742–5753.
71. Ohno, K.; Maeda, S. Global reaction route mapping on potential energy surfaces of formaldehyde, formic acid, and their metal-substituted analogues. *J. Phys. Chem. A* **2006**, *110*, 8933–8941.
72. Fernández, E.; Soler, J.M.; Garzón, I.L.; Balbás, L.C. Trends in the structure and bonding of noble metal clusters. *Phys. Rev. B* **2004**, *70*, 165403:1–165403:14.
73. Walker, A.W. Structure and energetics of small gold nanoclusters and their positive ions. *J. Chem. Phys.* **2005**, *122*, 094310:1–094310:12.
74. Xiao, L.; Tollberg, B.; Hu, X.; Wang, L. Structural study of gold clusters. *J. Chem. Phys.* **2006**, *124*, 094310:1–094310:10.
75. Häkkinen, H. Atomic and electronic structure of gold clusters: Understanding flakes, cages and superatoms from simple concept. *Chem. Soc. Rev.* **2008**, *37*, 1847–1859.
76. Sánchez-Portal, D.; Ordejón, P.; Artacho, E.; Soler, J.M. Density-functional method for very large systems with LCAO basis sets. *Int. J. Quantum Chem.* **1997**, *65*, 453–461.
77. Soler, J.M.; Artacho, E.; Gale, J.D.; García, A.; Junquera, J.; Ordejón, P.; Sánchez-Portal, D. The siesta method for ab initio order-N materials simulation. *J. Phys. Condens. Matter* **2002**, *14*, 2745–2779.
78. Sánchez-Portal, D.; Ordejón, P.; Canadell, E. Computing the properties of materials from first principles with siesta. *Struct. Bond.* **2004**, *113*, 103–170.
79. Bader, R. *Atoms in Molecules: A Quantum Theory*; Oxford University Press: New York, NY, USA, 1990.
80. Henkelman, G.; Arnaldsson, A.; Jònsson, H. A fast and robust algorithm for Bader decomposition of charge density. *Comput. Mater. Sci.* **2006**, *36*, 354–360.
81. Kokalj, A. Computer graphics and graphical user interfaces as tools in simulations of matter at the atomic scale. *Comput. Mater. Sci.* **2003**, *28*, 155–168.

82. Huber, K.P.; Herzberg, G. *Molecular Spectra and Molecular Structure Constants of Diatomic Molecules*; Van Nostrand Reinhold: New York, NY, USA, 1979.
83. Furthmüller, J.; Hafner, J.; Kresse, G. *Ab initio* calculation of the structural and electronic properties of carbon and boron nitride using ultrasoft pseudopotentials. *Phys. Rev. B* **1994**, *50*, 15606–15622.
84. Orellana, W.; Chacham, H. Stability of native defects in hexagonal and cubic boron nitride. *Phys. Rev. B* **2001**, *63*, 125205:1–125205:7.
85. Kuzubov, A.A.; Serzhantova, M.V.; Fedorov, A.S.; Tomilin, F.N.; Kozhevnikova, T.A. Theoretical study of vacancies and adatoms in white graphene. *JETP Lett.* **2011**, *93*, 335–338.
86. Si, M.S.; Li, J.Y.; Shi, H.G.; Niu, X.N.; Xue, D.S. Divacancies in graphitic boron nitride sheets. *Europhys. Lett.* **2009**, *86*, 46002:1–46002:6.
87. Zobelli, A.; Ewels, C.P.; Gloter, A.; Seifert, G.; Stephan, O.; Csillag, S.; Colliex, C. Defective structure of BN nanotubes: From single vacancies to dislocation lines. *Nano Lett.* **2006**, *6*, 1955–1960.
88. Jin, C.; Lin, F.; Suenaga, K.; Iijima, S. Fabrication of a freestanding boron nitride single layer and its defect assignments. *Phys. Rev. Lett.* **2009**, *102*, 195505:1–195505:4.
89. Yin, L.C.; Cheng, H.M.; Saito, R. Triangle defect states of hexagonal boron nitride atomic layer: Density functional theory calculations. *Phys. Rev. B* **2010**, *81*, 153407:1–153407:4.
90. Corso, M.; Auwärter, W.; Muntwiler, M.; Tamai, A.; Greber, T.; Osterwalder, J. Boron nitride nanomesh. *Science* **2004**, *303*, 217–220.
91. Laskowski, R.; Blaha, P.; Schwarz, K. Bonding of hexagonal BN to transition metal surfaces: An ab initio density-functional theory study. *Phys. Rev. B* **2008**, *78*, 045409:1–045409:10.
92. *Inorganic Chemistry*; Wiberg, N., Holleman, A.F., Wiberg, E., Eds.; Academic Press: Waltham, MA, USA, 2001.
93. Ramamoorthy, M.; Vanderbilt, D.; King-Smith, R.D. First-principles calculations of the energetics of stoichiometric TiO_2 surfaces. *Phys. Rev. B* **1994**, *49*, 16721–16727.
94. Perron, H.; Domain, C.; Roques, J.; Drot, R.; Simoni, E.; Catalette, H. Optimisation of accurate rutile TiO_2(110), (100), (101) and (001) surface models from periodic DFT calculations. *Theor. Chem. Acc.* **2007**, *117*, 565–574.
95. Lyalin, A.; Taketsugu, T. Catalitic activity of gold clusters. *AIP Conf. Proc.* **2009**, *1197*, 65–75.
96. Barrio, L.; Liu, P.; Rodríguez, J.A.; Campos-Martín, J.M.; Fierro, J.L.G. A density functional theory study of the dissociation of H_2 on gold clusters: Importance of fluxionality and ensemble effects. *J. Chem. Phys.* **2006**, *125*, 164715:1–164715:5.